

Electron Energy Loss Spectroscopy (EELS)

ME-228 Materials and Structure Property Correlations

Apratim Sanyal (6310-410-101-07511)

Mainak Kundu (6310-410-101-07598)

Samaresh Midya (6310-410-101-07682)

Electron Energy Loss Spectroscopy (EELS)

The Experiment: (HOW?)

Inelastic scattering of electrons or **Electron Energy Loss Spectroscopy (EELS)** is the most versatile technique for the investigation of vibrational modes on surfaces in vacuum. The energy resolution of present-day spectrometers is as high as 1 meV. All vibration modes from the low frequency vibrations of physisorbed rare-gas atoms to the internal vibrations of molecules are accessible in a single scan. Furthermore, one can probe phonons in the entire Brillouin zone. By varying the electron energy, different scattering mechanisms can be employed, leading to different selection rules for the inelastic scattering. In this first subsection, we discuss some of the salient properties of electron spectrometers that are used for inelastic electron scattering.

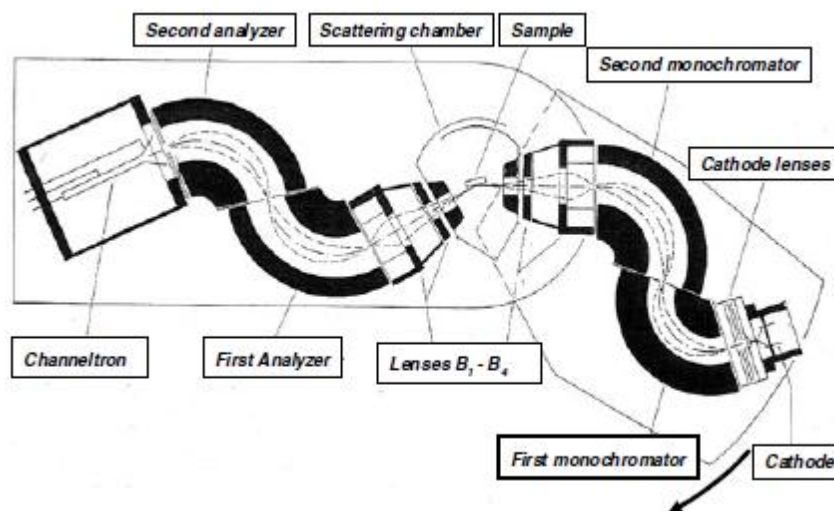


Figure 1: Electron spectrometer for inelastic scattering of electrons from surfaces.

The width of the energy distribution of electrons from thermal, field emission or photoemission cathodes is at least 200 meV. Energy selectors are required to make electrons useful for inelastic scattering from phonons. A second energy selector is required for the analysis of the scattered electrons. The combined resolution of the electron *monochromator* and *analyzer* must be in the low meV range. Electrostatic deflector type selectors, as opposed to magnetic deflectors are used exclusively, because of the difficulty to shield magnetic fields effectively. Figure 1 displays a typical experimental set-up of an electron spectrometer. It comprises the electron emission system, two monochromators, lenses to image the exit slit of the monochromator onto the sample and further onto the analyzer entrance slit, two analyzers and a channeltron electron multiplier. In the interest of an optimum intensity of the signal, perfect as possible images of each aperture onto the next one are required. Just as in light optics, the phase space is conserved in the process of imaging. Because of the C_{2v} symmetry of the optics around the beam direction, phase space conservation applies to the plane of drawing in Fig. 1 and perpendicular to the plane of drawing separately.

$$s \sin \alpha \sqrt{E} = \text{const.}$$

$$h \sin \beta \sqrt{E} = \text{const.}$$

Here, E is the beam energy, s and h are the width and heights of the slit apertures, and α and β are the angular apertures in the plane and perpendicular to the plane in Fig.1. The energy range of the electrons to be scattered at the sample is between a few and a few hundred eV. As the quantum energies of vibrational motions are a few hundred meV at the most, the energies of the inelastically scattered electrons are about the same as the energy of the incident electrons. Together with the condition of phase space conservation, this calls for an electron optics that is identical in the monochromator and the analyzer part, in reverse order. A small allowance may have to be made to match the electron optics of the monochromator to the tendency of high intensity beams to diverge because of the repulsive interaction between the electrons.

Classical energy dispersive deflectors are the spherical deflector, which ideally has stigmatic focusing for a total deflection angle of 180° and the cylindrical deflector that focuses in the plane perpendicular to the cylinder axis at 127° . Metallic plates at both ends with slit apertures to achieve energy selections reduce the focusing angles in both cases whereby the spherical deflector loses its perfect stigmatic focusing. For both devices, the basic equation that describes the image of the entrance slit at the exit-slit position is

$$y_{\text{exit}} = -y_{\text{entrance}} + c_D r_0 \delta E / E_p - c_{\alpha\alpha} r_0 \alpha^2 - c_{\beta\beta} r_0 \beta^2 .$$

Here, r_0 is the radius of the center path of the electron and y_{exit} and y_{entrance} are the deviations of the electron trajectory from the radius r_0 at the entrance and exit slits, respectively. E_p is the nominal pass energy for electrons traveling tangential to the radius r_0 , δE is the deviation from that energy, c_D is a constant describing the energy dispersion, α is the angle in the dispersion plane that the trajectory makes with the tangential path at the entrance slit, β is the corresponding angle perpendicular to the dispersion plane, and $c_{\alpha\alpha}$ and $c_{\beta\beta}$ are the second order angular aberrations in the dispersion plane and perpendicular to it, respectively. The first order term in α vanishes, as the devices possess first order focusing. The first order term in β vanishes for the spherical deflector because of symmetry. The constants $c_{\alpha\alpha}$, $c_{\beta\beta}$ and c_D are $4/3$, 1 and 1.0 for the cylindrical deflector, and 1 , 0 and 2.0 for the ideal spherical deflector.

With the improvements in computing power, bundles of electron trajectories are calculated within a short time even on a PC. This has opened the possibility to design free-form deflectors whose properties can be optimized with respect performance and ease of construction. The deflector that proved best in performance for the purpose of electron energy loss spectroscopy is illustrated in Fig.2.

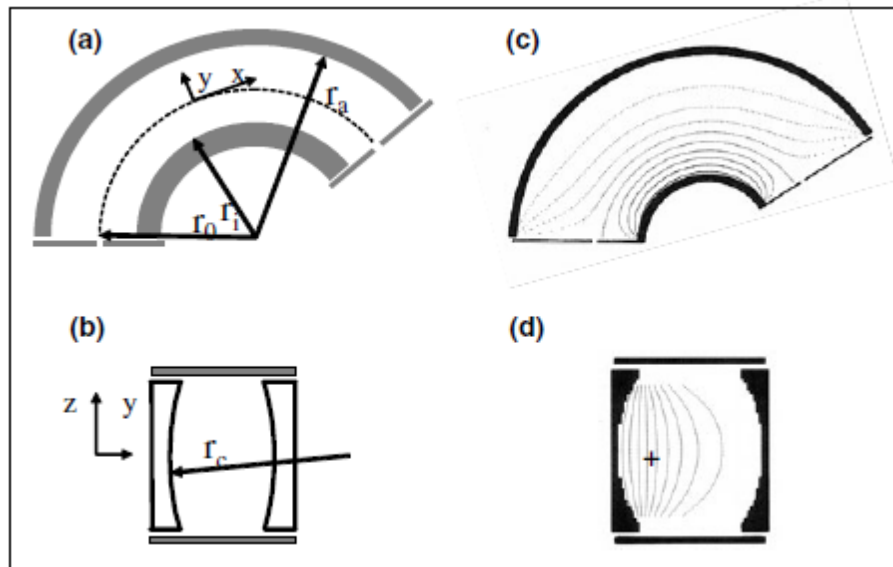


Figure 2: Free-form electrostatic deflector that features stigmatic focusing, equipotential metal apertures and a correction of the angular aberration in the dispersion plane. (a) Cross section in the dispersion plane showing the deflector plates and the entrance and exit apertures. (b) Cross section perpendicular to the electron path showing the concavely shaped deflector plates. (c, d) As (a) and (b), yet with the dashed equipotential lines obtained from the solution of the Laplace-equation for the device.

The cross section in the dispersion plane shows deflector plates that are curved as for a cylindrical deflector (2a). Orthogonal to the dispersion plane the deflector plates are concavely shaped (2b) with a radius of curvature r_c . Since the radial field is zero right after the entrance slit and right before the exit slit, electrons do not travel along the equipotential line that connects entrance and exit slit (2c),

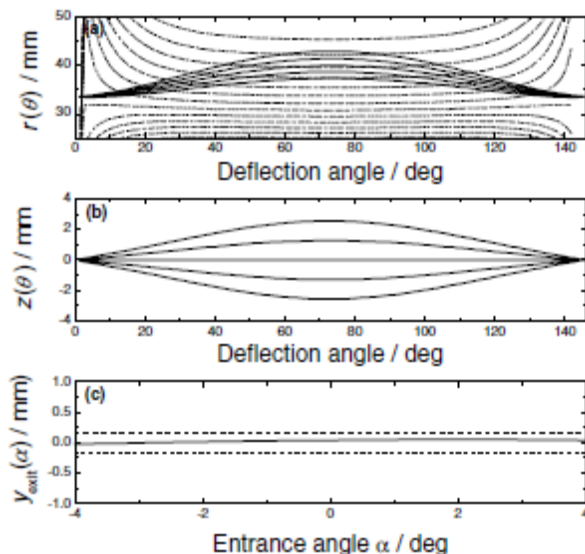


Figure 3: Electron trajectories in a free-form deflector of the type shown in Fig.2. Parameters are the radial position of the entrance slit $r_0 = 33.5$ mm, radii of inner and outer deflection plate $r_i = 20.5$ mm and $r_o = 60$ mm, respectively, and $r_c = 100$ mm. **(a)** Radial position $r(\theta)$ versus the deflection angle θ for the entrance angles $\alpha = -4^\circ, -2^\circ, 0^\circ, 2^\circ$ and 4° . **(b)** Position perpendicular to the dispersion plane $z(\theta)$ for the entrance angles $\beta = -4^\circ, -2^\circ, 0^\circ, 2^\circ$ and 4° . **(c)** Deviation of the radial position from r_0 at the exit slit as a function of the entrance angle α .

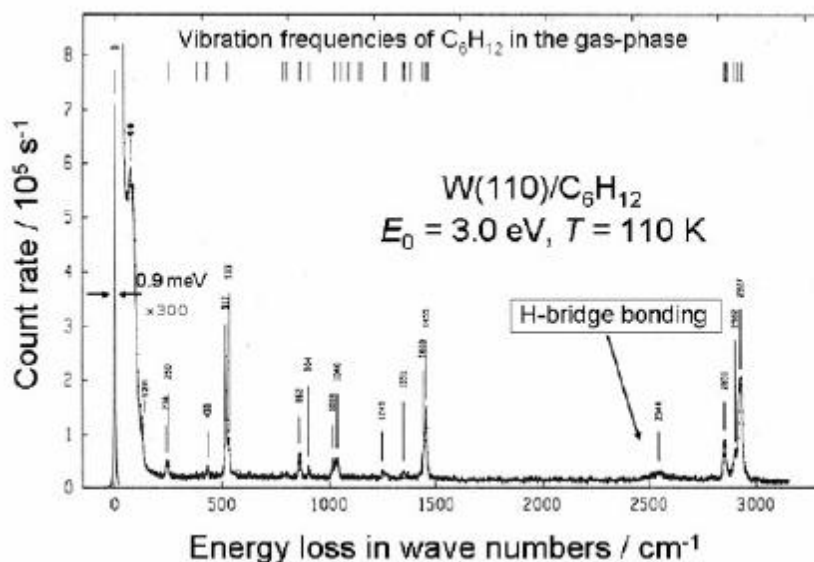


Figure 4: Electron energy loss spectrum of cyclohexane on W(110) showing the performance of advanced spectrometers. In addition to the gas-phase modes, the spectrum shows the shifted CH-stretching mode of the hydrogen atoms pointing towards the surface and surface induced splittings of the modes at 250 and 520 cm^{-1} .

but rather travel up to larger radii until midway of the path. This is illustrated in the upper panel Fig.3. The concave curvatures in combination with the top and bottom cover plates ensure the stigmatic focusing while minimizing

simultaneously the angular aberrations. The angular aberration in the dispersion plane can be reduced to zero, by making $r_c \approx 1.3r_0$. However, the sum of the angular aberration coefficients $c_{\alpha\alpha} + c_{\theta\theta}$ stays constant. In total, the device behaves nearly as an ideal sphere without fringe fields from the entrance and exit aperture. Unlike the ideal spherical deflector, the device is very robust with respect to high current loads. This is owed to the fact that the device has active stigmatic focusing whereas the ideal sphere has stigmatic focusing only because of the spherical symmetry. Figure 4 shows an example of a high-resolution spectrum obtained with the spectrometer featuring the free-form deflectors.

Theory of Inelastic Electron Scattering (WHAT & WHY?)

In inelastic scattering of electrons one distinguishes three types of mechanisms, scattering from long-range electric fields ("*dipole scattering*"), scattering from the short-range atomic potentials ("*impact scattering*"), and scattering via short lived resonances with molecular orbitals ("*resonance scattering*"). The mechanisms are illustrated in Fig. 5. Each mechanism has its own characteristic features, with respect to angular distribution of the scattered electrons, the dependence of the cross section on the electron energy, the selection rules that apply, and each mechanism requires a theory of its own. Resonance scattering, e.g. occurs in weakly bound molecules at particular electron energies. The electron is captured for a short time in a molecular orbit. After some time the molecule undergoes a Frank-Condon transition from the ionic state into the ground state and the electron is re-emitted. The trajectory of the emitted electron is determined entirely by the symmetry of the molecular orbit. As the final state of the molecule may be vibrationally excited, the energy of the emerging electron is correspondingly lower. Since resonance scattering is less important for surface vibration spectroscopy as an analytical tool, we focus on dipole and impact scattering in the following.

Dipole scattering - the dielectric theory of electron solid interaction

We consider the interaction of electrons with dipolar electric fields of elementary excitations at surfaces. The theory is not confined to vibration spectroscopy. It applies equally to other elementary excitations such as electronic transitions and plasma excitation in the limit of small momentum transfer. The theory of dipole scattering can be approached from three different viewpoints, each one having its own virtues and shortcomings. One possibility is to consider the Hamiltonian of the free electron and treat the dipole fields associated with the elementary excitations as a perturbation in the spirit of the Born-approximation. The advantage of this approach is that it delivers the scattering kinematics, i.e. energy and momentum conservation. The disadvantage is that one has to focus on a particular type of elementary excitation. The second approach considers the Hamiltonian of the excitation and treats the electron as an external perturbation. Because of the smallness of the momentum change involved in inelastic scattering from long-range dipole fields the electron trajectory can be assumed to be unperturbed by the inelastic event (Fig.5a). This treatment delivers the multiple losses straightforwardly. The disadvantage is that energy and momentum conservation have to be introduced ad hoc.

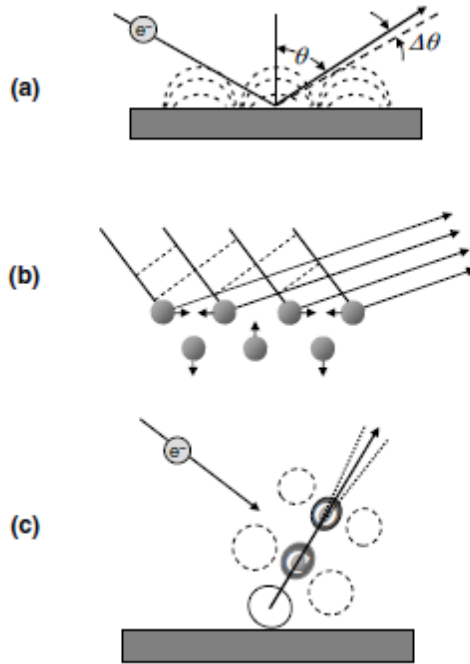


Figure 5: Illustration of the three different scattering mechanisms, which are operative at surfaces. Small-angle dipole scattering (a), wide-angle impact scattering (b), and resonance scattering (c).

The third possibility is to consider the inelastic interaction as a classical energy loss of a charged particle reflected from a surface. The advantage of the latter formulation is that it is independent of the specific elementary excitation. Solids and adsorbed species on solids are represented by their complex dielectric functions $\epsilon(\omega)$ and their complex dynamic polarizabilities $\alpha(\omega)$, respectively. In their specific realms of applicability, all three approaches lead to the same final expression for the inelastically scattered intensity. We pursue the third path in the following, usually known as the *dielectric theory* of inelastic electron scattering. As a matter of convenience, we do the derivation in Gaussian units. The theory was originally developed by Geiger and Raether for inelastic scattering of high-energy electrons in transmission geometry. The low energy reflection case was first studied by Lucas and Sunjic using the second approach. The quantum theory of scattering for the reflection geometry was developed by Evans and Mills.

In classical electrodynamics the total energy dissipation is

$$W = \frac{1}{4\pi} \int dt \int d^3r \mathcal{E}(\mathbf{r}, t) \cdot \dot{\mathbf{D}}(\mathbf{r}, t) \quad \dots(2)$$

Where $\mathcal{E}(\mathbf{r}, t)$ and $\dot{\mathbf{D}}(\mathbf{r}, t)$ are the electric field and the time derivative of the displacement, respectively. The integral extends over the entire space. By writing the energy loss that way, we have restricted our considerations to local and instantaneous dielectric responses. This approximation suffices in most cases of interest. We remark however that the surface response of metals due to electron-hole pair excitations is not properly described within the framework of local dielectric response. The total energy dissipation can also be expressed in terms of the probability $P(\mathbf{q}_{\parallel}, \omega)$ for an energy loss of energy $\hbar\omega$ and momentum $\hbar\mathbf{q}_{\parallel}$,

$$W = \int_{\hbar\omega > 0} d(\hbar\omega) d\mathbf{q}_{\parallel} \hbar\omega P(\mathbf{q}_{\parallel}, \omega) \quad \dots(1)$$

For surface losses, one may employ the two-dimensional Fourier expansion

$$\mathcal{E}(\mathbf{r}, t) = \int d\omega d\mathbf{q}_{\parallel} e^{-i\omega t} e^{i\mathbf{q}_{\parallel} \cdot \mathbf{r}_{\parallel}} e^{-q_{\parallel}|z|} \mathcal{E}(\mathbf{q}_{\parallel}, z, \omega)$$

Here the position vector is $\mathbf{r} = (\mathbf{r}_{\parallel}, z)$, and the surface plane is at $z = 0$. The expansion may be considered as an expansion into dielectric surface. The integral extends over negative and positive ω . An analogous expansion holds for the displacement $\mathbf{D}(\mathbf{r}, t)$. The Fourier-components of \mathbf{D} and \mathcal{E} are related to each other by the dielectric function $\epsilon(\omega) = \epsilon_1(\omega) + i\epsilon_2(\omega)$, which we assume to be scalar for the moment. A possible dependence on \mathbf{q}_{\parallel} can be neglected as the scattering process is near $\mathbf{q}_{\parallel} = 0$, but still to the far-right of the light line. By inserting above eqn and the corresponding equation for the displacement $\mathbf{D}(\mathbf{r}, t)$ into eqn for total energy dissipation and by considering that the integrals

$$\int_{-\infty}^{\infty} dx e^{i(q-q')x} = 2\pi\delta(q-q')$$

$$\int_{-\infty}^{\infty} dt e^{i(\omega-\omega')t} = 2\pi\delta(\omega-\omega')$$

are representations of delta-function, one obtains the expansion for the energy loss

$$W = 2\pi^2 \int d\omega d\mathbf{q}_{\parallel} \omega \epsilon_2(\omega) \int_{z \leq 0} dz z \left| \mathcal{E}_{\text{int}}(\mathbf{q}_{\parallel}, z, \omega) \right|^2 e^{-2q_{\parallel}|z|}$$

As the imaginary part of $\epsilon(\omega)$ is zero in vacuum, only the electric field inside the material $\mathcal{E}_{\text{int}}(\mathbf{q}_{\parallel}, z, \omega)$ matters and the integral extends only over the half-space $z \leq 0$. The integral over \mathbf{q}_{\parallel} and ω has the form of (1). The integral over z is therefore the loss probability $P(\mathbf{q}_{\parallel}, \omega)$. The internal electric field is generated by the electron while it is approaching the surface from the outside and after it is reflected from the surface potential barrier or diffracted by the near-surface atoms. The electron also spends a short time inside the solid before it emerges in the vacuum again. For low energy electrons with their small penetration depth, this part may be neglected. The internal electric field therefore stems from a charge outside the solid. If the solid is a semi-infinite dielectric half-space in $z \leq 0$, the relation between the internal field $\mathcal{E}_{\text{int}}(\mathbf{q}_{\parallel}, z, \omega)$ and an external field $\mathcal{E}_{\text{ext}}(\mathbf{q}_{\parallel}, z, \omega)$ is

$$\mathcal{E}_{\text{int}}(\mathbf{q}_{\parallel}, z, \omega) = \frac{2\mathcal{E}_{\text{ext}}(\mathbf{q}_{\parallel}, z, \omega)}{\epsilon(\omega) + 1}$$

The loss probability is therefore proportional to

$$P(\mathbf{q}_{\parallel}, \omega) \propto \frac{\epsilon_2(\omega)}{|\epsilon(\omega) + 1|^2} = \text{Im} \frac{-1}{\epsilon(\omega) + 1}$$

The loss probability has a pole at the frequency of the dielectric surface wave. As an example, we consider the dielectric function of an infrared active material in the case of small damping γ .

$$\epsilon(\omega) = \epsilon_{\infty} + \frac{\omega_0^2 (\epsilon_{\text{st}} - \epsilon_{\infty})}{\omega_0^2 - \omega^2 - i\gamma\omega}$$

Then

$$P(\mathbf{q}_{\parallel}, \omega) \propto \lim_{\gamma \rightarrow 0} \text{Im} \frac{-1}{\epsilon(\omega) + 1} = \frac{\epsilon_{\text{st}} - \epsilon_{\infty}}{(1 + \epsilon_{\text{st}})(1 + \epsilon_{\infty})} \frac{\pi\omega_s}{4} \delta(\omega - \omega_s)$$

With

$$\omega_s = \omega_0 \left(\frac{1 + \epsilon_{\text{stat}}}{1 + \epsilon_{\infty}} \right)^{1/2}$$

the frequency of the Fuchs-Kliwler surface phonon. We thus learn that surface phonons are excited by electrons while the electrons are outside the solid; longitudinal bulk phonons are excited by electrons inside the solid since the screening factor is $1/\epsilon(\omega)$ in that case. The same holds for plasmon excitations.

We now consider the case of a thin dielectric layer of thickness d on a nonabsorbing substrate. The substrate/layer interface is at $z = 0$. The dielectric functions of layer and substrate are denoted as $\epsilon_s(\omega)$ and ϵ_b , respectively. It is assumed that $|\epsilon_s(\omega) q_{||} d| \ll \epsilon_b$. The potential ϕ originating in a charged particle outside the solid is as if the layer did not exist. The potential is given by the potential of the bare charge and the image charge inside the solid

$$\phi(\mathbf{r}) = \frac{e}{r} - \frac{\epsilon_b - 1}{\epsilon_b + 1} \frac{e}{r'}$$

where \mathbf{r} and \mathbf{r}' are the vectors pointing from the charge and its image to a particular point (Fig.6)

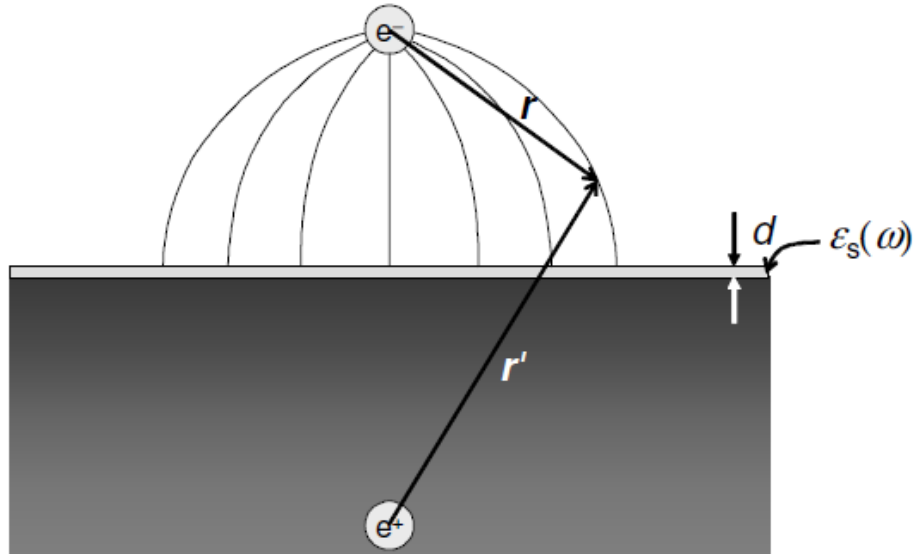


Fig.6. Electric field lines of a point charge near a surface of a dielectric material with a dielectric permeability $\epsilon_b \gg 1$. The dielectric active surface layer is assumed thin so that the field is not affected by the presence of the layer.

To calculate the dielectric losses of the active layer we make use of the fact that the parallel component of the electric field and the normal component of the displacement are continuous at the interface to the substrate and remain constant in the thin active layer. We rewrite the scalar product $\mathcal{E} \cdot \dot{\mathbf{D}}$ under the integral (2) as

$$\mathcal{E} \cdot \dot{\mathbf{D}} = \epsilon_{s||} \mathcal{E}_{||} \cdot \dot{\mathcal{E}}_{||} + \frac{1}{\epsilon_{s\perp}} D_{\perp} \dot{D}_{\perp}$$

and thereby admit a tensorial dielectric function ϵ_s inside the active layer. The parallel component of the electric field $\mathcal{E}_{||}$ is

$$\mathcal{E}_{||} \Big|_{z=0} = -e \nabla_{||} \left(\frac{e}{r} + \frac{1 - \epsilon_b}{1 + \epsilon_b} \frac{e}{r'} \right) \Big|_{z=0} = -\frac{2}{1 + \epsilon_b} \nabla_{||} \frac{e}{r} \Big|_{z=0} = \frac{2}{1 + \epsilon_b} \mathcal{E}_{\text{bare||}}$$

where $\mathcal{E}_{\text{barell}}$ is the field of the electron charge at the interface $z = 0$ without the image charge. Note that

$$\nabla_{\parallel} r^{-1} = +\nabla_{\parallel} r'^{-1} \text{ but } \nabla_z r^{-1} = -\nabla_z r'^{-1} \text{ at } z = 0$$

The vertical component of the displacement D_{\perp} is

$$\begin{aligned} D_{\perp}|_{z=0} &= -e\epsilon_b \nabla_z \left(\frac{e}{r} + \frac{1-\epsilon_b}{1+\epsilon_b} \frac{e}{r'} \right) \Big|_{z=0} \\ &= -\frac{2\epsilon_b}{1+\epsilon_b} \nabla_z \frac{e}{r} \Big|_{z=0} = \frac{2\epsilon_b}{1+\epsilon_b} \mathcal{E}_{\text{bare}\perp} \end{aligned}$$

The total energy loss expressed in terms of the Fourier-components thereby becomes

$$\begin{aligned} W = 8\pi^2 d \int \omega d\omega d\mathbf{q}_{\parallel} \left[\frac{\text{Im} \epsilon_{\text{sll}}(\omega)}{(\epsilon_b + 1)^2} \left| \mathcal{E}_{\text{barell}}(\mathbf{q}_{\parallel}, z = 0, \omega) \right|^2 \right. \\ \left. - \frac{\epsilon_b^2}{(\epsilon_b + 1)^2} \text{Im} \frac{1}{\epsilon_{\text{s}\perp}(\omega)} \left| \mathcal{E}_{\text{bare}\perp}(\mathbf{q}_{\parallel}, z = 0, \omega) \right|^2 \right] \end{aligned} \quad \text{.....(3)}$$

For substrates with $|\epsilon_b| \gg 1$, hence in particular for metal surfaces, only the term with the perpendicular component of the field survives which constitutes the surface selection rule. The dielectric active surface layer is frequently a monolayer of molecules with dipole active vibration modes. In that case

$$d \text{Im} \frac{1}{\epsilon_{\text{s}\perp}(\omega)} \cong 4\pi n_s \text{Im} \alpha_{\text{s}\perp}(\omega) \quad \text{.....(5)}$$

where $\alpha_{\text{s}\perp}(\omega)$ is the dynamic polarizability of the molecule and n_s is the surface density. In order to express the integrand of (3) (which is $P(\mathbf{q}_{\parallel}, \omega)$) in terms of the scattering parameters we need the Fourier-transform of the potential $e/r(t)$,

$$\frac{e}{r} = \frac{e}{2\pi} \int d\mathbf{q}_{\parallel} \frac{1}{q_{\parallel}} e^{-q_{\parallel}|z|} e^{-i\mathbf{q}_{\parallel} \cdot \mathbf{r}_{\parallel}}$$

The gradient of the potential, the electric field, has therefore the expansion

$$-\nabla \frac{e}{r} = \frac{e}{2\pi} \int d\mathbf{q}_{\parallel} (i\mathbf{e}_{\parallel}, 1) e^{-q_{\parallel}|z|} e^{-i\mathbf{q}_{\parallel} \cdot \mathbf{r}_{\parallel}}$$

in which $(i\mathbf{e}_{\parallel}, 1)$ is a three dimensional vector with the perpendicular component 1 and \mathbf{e}_{\parallel} the unit vector in the surface plane.

We now study the probability for a phonon excitation for an electron that is reflected at the surface at the time $t = 0$. In that case

$$\mathbf{r}(t) = \mathbf{r}_{\parallel} + v_{\parallel} t \mathbf{e}_{\parallel} + v_{\perp} |t| \mathbf{e}_{\perp} \quad -\infty < t < \infty ,$$

where v_{\parallel} and v_{\perp} are the electron velocities parallel and perpendicular to the surface, respectively. The vector \mathbf{r}_{\parallel} has its origin in the point of reflection and points to an arbitrary position on the surface. The Fourier-integral of the electric field is

$$\begin{aligned} \mathcal{E}_{\text{bare}}(\mathbf{r}, t) &= -\nabla \frac{e}{|\mathbf{r}_{\parallel} + v_{\parallel} t \mathbf{e}_{\parallel} + v_{\perp} |t| \mathbf{e}_{\perp}|} \\ &= \frac{1}{2\pi} \int d\mathbf{q}_{\parallel} (i\mathbf{e}_{\parallel}, 1) e^{-i(\mathbf{q}_{\parallel} \cdot (\mathbf{r}_{\parallel} + v_{\parallel} t))} e^{-q_{\parallel} (|z| + v_{\perp} |t|)} \end{aligned}$$

The Fourier integral of the kernel with respect to time is

$$e^{-i\mathbf{q}_{\parallel} \cdot \mathbf{v}_{\parallel} t} e^{-q_{\parallel} v_{\perp} |t|} = \frac{1}{2\pi} \int d\omega e^{-i\omega t} \frac{2q_{\parallel} v_{\perp}}{(\omega - \mathbf{q}_{\parallel} \cdot \mathbf{v}_{\parallel})^2 + q_{\parallel}^2 v_{\perp}^2} .$$

The Fourier-components of the electric field are therefore

$$\mathcal{E}_{\text{bare}}(\mathbf{q}_{\parallel}, \omega) = (i\mathbf{e}_{\parallel}, 1) \frac{e}{(2\pi)^2} \frac{2q_{\parallel} v_{\perp}}{(\omega - \mathbf{q}_{\parallel} \cdot \mathbf{v}_{\parallel})^2 + q_{\parallel}^2 v_{\perp}^2}$$

By inserting this equation into (3) and comparing with (1) we obtain the probability for the reflected electron to suffer an energy loss of $\hbar\omega$ with a wave vector \mathbf{q}_{\parallel} .

$$P(\mathbf{q}_{\parallel}, \omega) = \frac{16e^2 n_s}{\hbar^2 \pi} \frac{q_{\parallel}^2 v_{\perp}^2}{((\omega - \mathbf{q}_{\parallel} \cdot \mathbf{v}_{\parallel})^2 + q_{\parallel}^2 v_{\perp}^2)^2} \text{Im} \alpha_{s\perp}(\omega)$$

.....(4)

The probability has a sharp resonance at the *surfing condition*

$$v_{\parallel} = \omega / q_{\parallel} .$$

The resonance is infinitely sharp (is this approximation) for grazing incidence. Because of wave vector conservation, the surfing condition entails that the electrons are scattered into a small angular cone around all the directions of elastic scattering, around the specular reflected beam as well as around the diffracted beams. In either case, the intensity of the inelastically scattered electrons is proportional to the elastic intensity. In practical applications of (4), one is interested in the inelastically scattered intensity observed in a small angular aperture. The aperture angles of spectrometers are small because of angular aberrations in the deflectors and in the lens systems. We denote the angular deviations from the specular beam in the scattering plane and perpendicular to it as α and β , respectively.

From momentum conservation one obtains

$$q_{\parallel x} \cong -\frac{\sqrt{2mE_1}}{\hbar}(\alpha \cos \theta_1 + \vartheta_E \sin \theta_1)$$

$$q_{\parallel y} \cong \frac{\sqrt{2mE_1}}{\hbar} \beta$$

$$\text{with } \vartheta_E = \hbar\omega / 2E_1, \alpha, \beta \ll 1$$

where E_1 is the energy of the incident electron. The condition $\vartheta_E \ll 1$ is consistent with the initial assumption that the trajectory of the electron should remain essentially unaffected by the inelastic scattering process. The element in \mathbf{q}_{\parallel} -space is converted into the angular space by

$$d\mathbf{q}_{\parallel} = k_1^2 \cos \theta_1 d\alpha d\beta$$

where k_1 is the wave vector of the incident electron. We introduce furthermore reduced angles as

$$\hat{\alpha} = \alpha / \vartheta_E, \hat{\beta} = \beta / \vartheta_E.$$

With these notations, one obtains the relative intensity of inelastic events as

$$\frac{dI_{\text{inel}}}{I_{\text{el}} d\hbar\omega} = \frac{8n_s \text{Im}\alpha_{s\perp}(\omega)}{\pi a_B E_1 \cos \theta_1} [1+n(\omega)] \int_{-\hat{\alpha}_c}^{\hat{\alpha}_c} d\hat{\alpha} \int_{-\hat{\beta}_c}^{\hat{\beta}_c} d\hat{\beta} \frac{(\hat{\alpha} \cos \theta_1 + \sin \theta_1)^2 + \hat{\beta}^2}{(1+\hat{\alpha}^2 + \hat{\beta}^2)^2}$$

Here, $\hat{\alpha}_c$ and $\hat{\beta}_c$ are the aperture angles of the spectrometer and a_B is the Bohrradius. To account for the quantum statistics (not reproduced in the classical derivation) we have added the term $[1+n(\omega)]$ in which $n(\omega)$ is the boson occupation number of a harmonic oscillator of frequency ω . For energy gains, the factor $[1+n(\omega)]$ is replaced by $n(\omega)$.

Above form is suitable for numerical calculations of the intensity for a given oscillator strength of the vibration, once the angular apertures of the spectrometer are known. For an estimate of the intensity it is useful to integrate above under the assumption of a circular aperture. With the transformation into polar coordinates

$$\hat{\alpha} = \hat{\vartheta} \cos \varphi \quad \hat{\beta} = \hat{\vartheta} \sin \varphi$$

one obtains after some algebra

$$\frac{dI_{\text{inel}}}{I_{\text{el}} d\hbar\omega} = \frac{4n_s \text{Im}\alpha_{s\perp}(\omega)}{a_B E_1 \cos \theta_1} [1+n(\omega)] \times \left[(\sin^2 \theta_1 - 2 \cos^2 \theta_1) \frac{\hat{\vartheta}_c^2}{1+\hat{\vartheta}_c^2} + (1+\cos^2 \theta_1) \ln(1+\hat{\vartheta}_c^2) \right]$$

In the limit $\hat{\vartheta}_c \ll 1$ that is typical for energy losses due to innermolecular vibrations the intensity is

$$\frac{dI_{\text{inel}}}{I_{\text{el}} d\hbar\omega} = \frac{32 E_1}{a_B (\hbar\omega)^2} \frac{\sin^2 \theta_1}{\cos \theta_1} [1+n(\omega)] \hat{\vartheta}_c^2 n_s \text{Im}\alpha_{\perp}(\omega)$$

The intensity of dipolar excitations, vibrational as well as electronic excitations, therefore falls off for higher frequencies. This explains why electronic transitions, e.g. interband transitions are very weak features in an energy loss spectrum. The frequency dependence of the intensity is in remarkable contrast to infrared absorption

spectroscopy. It is occasionally useful to express $\text{Im}\alpha_{s,\perp}(\omega)$ in terms of an effective charge e_{eff} associated with a mode. The dielectric function of a medium with a density n of harmonic oscillators in Gaussian units has the form

$$\varepsilon(\omega) = \varepsilon_{\infty} + \frac{4\pi e_{\text{eff}}^2 n / m_{\text{red}}}{\omega_0^2 - \omega^2 - i\gamma\omega}$$

in which m_{red} is the reduced mass. For a dilute layer $\varepsilon_{\infty}=1$. In the SI-system, the factor 4π is to be replaced by $1/\varepsilon_0$. Using the identity

$$\lim_{\gamma \rightarrow 0} \text{Im} \frac{1}{z - i\gamma} = \pi \delta(z)$$

one obtains with (5)

$$\text{Im} \alpha_{s,\perp}(\omega) = \frac{\pi}{2} \frac{n_s e_{\text{eff}}^2}{\varepsilon_{\infty}^2 m_{\text{red}} \omega_{\text{R}}} \delta(\omega_{\text{R}} - \omega) \quad \text{with} \quad \omega_{\text{R}}^2 = \omega_0^2 + 4\pi n e_{\text{eff}}^2 / m_{\text{red}}$$

Impact scattering

The Born approximation serve as a starting point for a treatment of the impact scattering. Inserting initial and final states of the solid expanded into phonon creation and annihilation operators yields the momentum conservation law for the components parallel to the surface and an expression for the inelastic crosssection in terms of the scattering potential. The salient features of this so-called *kinematic scattering theory* are more easily derived by considering the scattering of a classical wave from an arrangement of point scatterers. One can write the scattering amplitude as

$$f = f_0 e^{-i\omega_0 t} \sum_{l_{\parallel}, l_z, \mathbf{K}} e^{-i\mathbf{K} \cdot \mathbf{r}(l_{\parallel}, l_z, \mathbf{K}, t)}$$

in which \mathbf{K} is the difference between the wave vector of the incident wave k_i and the scattered wave k_s . The time dependent position vectors of the scattering centers $\mathbf{r}(l_{\parallel}, l_z, \mathbf{K}, t)$ can be expanded for small phonon amplitudes $\mathbf{u}(l_{\parallel}, l_z, \mathbf{K}, t)$

$$\mathbf{r}(l_{\parallel}, l_z, \mathbf{K}, t) = \mathbf{r}_0(l_{\parallel}, l_z, \mathbf{K}) + \mathbf{u}_0(q_{\parallel}, l_z, \mathbf{K}) e^{\pm i(q_{\parallel} r_0(l_{\parallel}, l_z, \mathbf{K}) - \omega(q_{\parallel})t)}$$

With this expansion the scattering amplitude becomes

$$f = f_0 e^{-i\omega_0 t} \delta(\mathbf{K}_{\parallel}) \sum_{l_z, \mathbf{K}} e^{-i\mathbf{K} \cdot \mathbf{r}(0l_z, \mathbf{K})} \\ + f_0 e^{-i(\omega_0 \pm \omega(q_{\parallel}))t} \delta(\mathbf{K}_{\parallel} \mp q_{\parallel}) \sum_{l_z, \mathbf{K}} \mathbf{K} \cdot \mathbf{u}_0(q_{\parallel}, l_z, \mathbf{K}) e^{-i\mathbf{K} \cdot \mathbf{r}(0l_z, \mathbf{K})}$$

in which the second term describes the classical analogue of inelastic scattering with energy and momentum conservation. The δ -functions result from the summation over l_{\parallel} . The scalar product of \mathbf{K} and

u_o vanishes if the displacements are perpendicular to the scattering plane, or more generally phrased, if the mode is odd with respect to the scattering plane. The energy dependence of the inelastically scattered intensity is given by the product

$$(\mathbf{K} \cdot \mathbf{u}_o)^2 \propto E_I$$

and the energy dependence of the atomic form factor $f_o(E_I)$. Neglecting the latter, the intensity of phonon scattering should be roughly proportional to the energy of the incident electron beam, i.e. a smooth function of the energy. The kinematic model would furthermore predict that the intensity of a phonon that is polarized parallel to the surface should be much less than the intensity of a perpendicular polarized phonon, since the vertical component of \mathbf{K} is much larger than the parallel component.

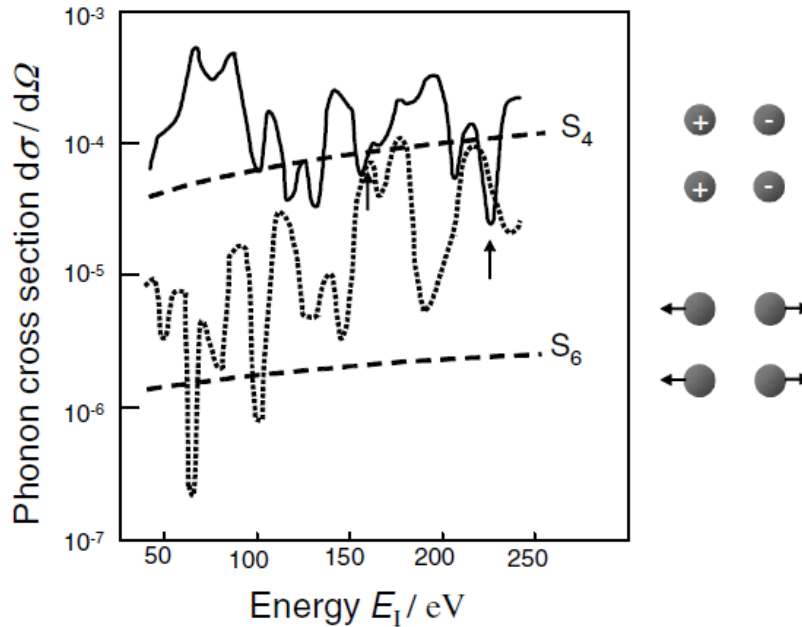


Fig.7. Calculated cross section for inelastic scattering from the S_4 and S_6 -phonon at X on the Ni(100) surface as function of the energy of the incident electron beam (solid and dashed lines respectively). The polar angle of detection is fixed to $\theta_S = 65^\circ$. The angle of the incident beam is adjusted to keep the momentum transfer at X. The arrows point to energies at which the intensity of the S_6 -phonon exceeds the intensity of the S_4 -phonon. The dashed lines mark the intensities according to the kinematic theory.

The kinematic scattering theory described above assumes that electrons are scattered only once whereas in reality low energy electrons scatter many times elastically before they emerge in a diffracted beam. A proper treatment of inelastic phonon scattering requires the consideration of these the multiple elastic scattering events. The *dynamic theory of scattering from phonons* has been worked out by Tong et al. in 1980. With multiple elastic scattering included, the cross sections become a strongly oscillating function of energy. This is illustrated in Fig.7 for the S_4 and S_6 -phonon on the Ni(100) at the X-point of the SBZ. The kinematic model predicts that the intensity of the S_6 -phonon should be almost two orders of magnitude lower than the intensity of the S_4 -phonon. This is also the overall trend according to the dynamic scattering theory. However, the strong oscillations effect that the intensity of the S_6 -phonon exceeds the intensity of the S_4 -phonon at certain energies (arrows in Fig.7). Experiments have confirmed the predictions of the theory. From the standpoint of an experimentalist, the strong oscillations in the cross section are an advantage as they enable the observation of modes polarized in the surface plane. Furthermore, one can distinguish phonons that have only a very small difference in energy, below the resolution of the spectrometer, by their different energy dependence of the cross section. This greatly expands the possibilities of inelastic electron scattering for the investigation of surface phonon dispersion.

Application: (WHERE?)

1) Thickness measurements

EELS allows quick and reliable measurement of local thickness in transmission electron microscope. The most efficient procedure is the following:

- Measure the energy loss spectrum in the energy range about -5..200 eV (wider better). Such measurement is quick (milliseconds) and thus can be applied to materials normally unstable under electron beam.
- Analyse the spectrum: (i) extract zero-loss peak (ZLP) using standard routines; (ii) calculate integrals under the ZLP (I_0) and under the whole spectrum (I).
- The thickness t is calculated as $\text{mfp} \cdot \ln(I/I_0)$. Here mfp is the mean free path of electron inelastic scattering, which has recently been tabulated for most elemental solids and oxides.

The spatial resolution of this procedure is limited by the plasmon localization and is about 1 nm, meaning that spatial thickness maps can be measured in scanning transmission electron microscope with ~ 1 nm resolution.

2) Pressure measurements

The intensity and position of low-energy EELS peaks are affected by pressure. This fact allows mapping local pressure with ~ 1 nm spatial resolution.

- **Peak shift method** is reliable and straightforward. The peak position is calibrated by independent (usually optical) measurement using a diamond anvil cell. However, the spectral resolution of most EEL spectrometers (0.3-2 eV, typically 1eV) is often too crude for the small pressure-induced shifts. Therefore, the sensitivity and accuracy of this method is relatively poor. Nevertheless, pressures as small as 0.2 GPa inside helium bubbles in aluminum have been measured.
 - **Peak intensity method** relies on pressure-induced change in the intensity of dipole-forbidden transitions. Because this intensity is zero for zero pressure the method is relatively sensitive and accurate. However, it requires existence of allowed and forbidden transitions of similar energies and thus is only applicable to specific systems, e.g., Xe bubbles in aluminum.
- 3) Study of silicate material for solar cells at a three millivolt resolution under EELS, allowed the identification of the vibrational modes of the phonon excitations. Although a large $10\mu\text{m}$ diameter beam was needed, the locally built monochromator and spectrometer, operating at 30 keV, allowed the transverse acoustic, transverse optical, longitudinal optical, rocking, stretching, wagging and bending modes all to be distinguished as separate peaks in the EELS spectrum. The effects of hydrogenation and preparation conditions were investigated.

4) Study of Interfaces—inner shells

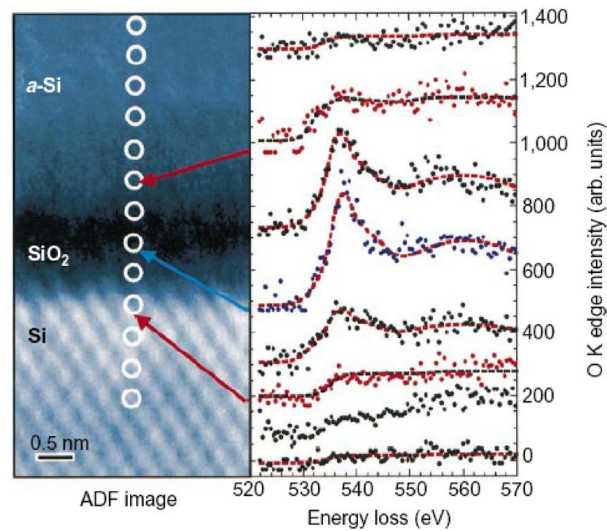


Figure 8. EELS of the oxygen K edge, mapped across a single transistor gate oxide interface. The spectra change as the local bonding of the oxygen atoms changes from that of interfacial states at the Si/SiO₂ boundary, to that of glassy silicon dioxide (middle), finally disappearing in the amorphous silicon (above). Exposure time—4 s per spectrum. Spatial resolution—0.26 nm, limited by the delocalization effects discussed in section.

Bibliography:

- 1) Physics of Surfaces and Interfaces by Harald Ibach
- 2) Absorption spectroscopy with sub-angstrom beams: ELS in STEM by John C H Spence
- 3) http://en.wikipedia.org/wiki/Electron_energy_loss_spectroscopy